Strain-Controlled Tensile Deformation Behavior of Isotactic Poly(1-butene) and Its Ethylene Copolymers

M. Al-Hussein* and G. Strobl

Fakultät für Physik, Albert-Ludwigs-Universität, Hermann-Herder-Str. 3, 79104 Freiburg, Germany

Received May 28, 2002; Revised Manuscript Received August 1, 2002

ABSTRACT: The tensile deformation behavior of poly(1-butene) and two of its ethylene copoloymers was studied at room temperature. This was done by investigating true stress−strain curves at constant strain rates, elastic recovery properties, and in-situ WAXS patterns during the deformation process. All samples showed a common rubberlike deformation behavior without necking down. The differential compliance, the recovery properties, and the evolution of the crystallite texture changed simultaneously at well-defined points. The strains at which these points occurred along the true stress−strain remained constants for the different samples despite their different percentage crystallinities. The same strain-controlled deformation behavior was also shown by a series of semicrystalline polymers in previous studies that carried out in our group. The well-defined way that the different samples respond to external stresses complies with our views of a granular substructure of the crystalline lamellae in a semicrystalline polymer as a result of the multistep route they follow during their formation.

1. Introduction

The plastic deformation behavior of a large number of semicrystalline polymers has been studied by many workers.[1−8] Upon such a deformation the initial isotropic structure is transformed into a highly anisotropic fibrillar one due to preferential orientation of the molecular chains. The mechanisms of this transformation and how they are related to the initial structure are of scientific interest. It also results in a considerable enhancement of the mechanical properties along the deformation direction so it is technologically important, too.[9−11] The overall conclusion that can be drawn from the different studies in the literature is that the deformation behavior of each semicrystalline polymer depends on several factors such as morphology, molecular orientation, percentage crystallinity, molecular weight, and drawing conditions in a rather complex manner. This gave the impression that a general simple law that can explain the deformation behavior of most semicrystalline polymers is virtually inconceivable.

The primary reason for such apparent complex behavior is due to the fact that most of these studies were based mainly on analyzing the nominal stress−strain curves.[1,2,7,8] It is known that most of semicrystalline polymers deform inhomogeneously, whereby a mechanical instability (e.g., a neck) develops at a certain position along the test specimen during the deformation. Once this instability has been developed, the test specimen no longer has a uniform width and so the stress and strain are not uniform along the whole test specimen. Consequently, the nominal stress and strain become involved properties. Stresses and strains must be examined locally in this case. This results in true values of the stress and strain which can then be used for a meaningful analysis. Experimentally, this can be done by devising a technique that enables the measurements to be confined to a small volume of the test specimen in which the strain can be assumed uniform. The other possibility to obtain a true stress−strain curve is when the test specimen deforms in a homogeneous manner.

In previous papers, we reported on the deformation behavior of several semicrystalline polymers based upon measurements of true stress−strain curves, elastic−recovery properties, and texture changes at different stages of the deformation process.[12,13] The results showed that there is indeed a general simple behavior that governs the deformation behavior of all the semicrystalline polymers that we have studied so far. The main characteristic of this "universal" behavior is the fact that it is controlled by strain rather than stress. Along the true stress−strain curve, the differential compliance, the recovery properties, and the crystallite texture change simultaneously at well-defined points. The strains at which these points take place are invariant over various strain rates, drawing temperatures, and crystallization temperatures. In contrast to this, the corresponding stresses vary considerably.

Table 1. Sample Characteristics

sample	grade	ethylene %	T_m/°C	crystallinity/%
A	PB0300	0	123	47
B	PB8220	2	119	37
C	PB010	>6	108	16

In a previous study, we have found that the same general behavior was shown by a set of polyethylene-based samples with various percentage crystallinities.[14] In this work, we have studied the effect of percentage crystallinity for another set of poly(1-butene)-based samples. Poly(1-butene) (P1B) is important mechanically, and it is renowned for its excellent creep resistance and the retaining of its mechanical properties at elevated temperatures.[15,16] It also can develop several crystalline forms depending on the crystallization conditions. It crystallizes from the melt in a tetragonal form II, which slowly transforms to the stable hexagonal form I. This transformation alters the properties of the material and can be assisted by applying an external stress.[17,18]

2. Experimental Section

2.1. Sample Characteristics and Preparation. Three different P1B-based samples were used in this study. They were kindly provided by Basell, Louvain-La-Neuva, Belgium, and their characteristics are shown in Table 1. Isotropic compression-molded sheets were prepared first from the

10.1021/ma020831k CCC: $22.00
Published on Web 09/24/2002

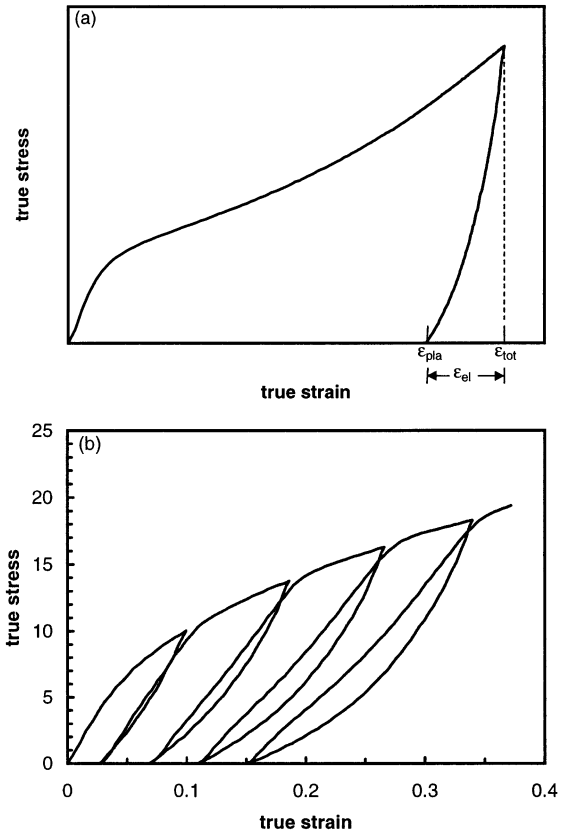

Figure 1. A representative example of the step−cycle test.

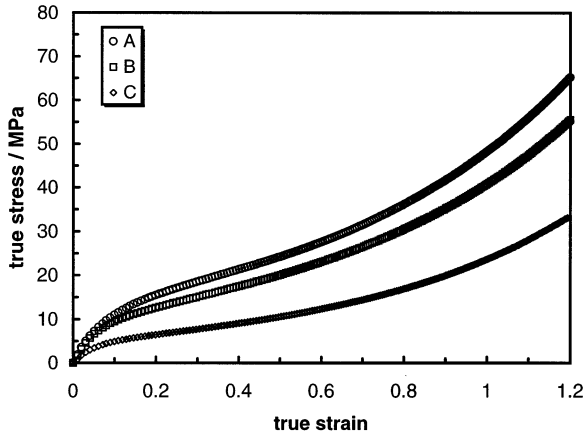

Figure 2. True stress−strain curves obtained at true strain rate of 0.005 s^{-1} of samples A, B, and C.

different samples with 0.3−0.5 mm thickness. This was done by melting a small quantity of pellets between two aluminum plates at 190 °C for 10 min under a slight pressure of 0.08 MPa. Then the pressure was increased to 0.63 MPa for another 10 min. The sheets were then left to cool slowly to room temperature. After that the sheets were stored at room temperature for at least 40 days to allow the samples to transform into their stable form I. Dog-bone-shaped specimens of gauge dimensions 6.5 × 4 mm were cut from the isotropic sheets for further drawing. The melting temperatures and percentage crystallinity values shown in Table 1 were obtained from DSC measurements. The percentage crystallinity values were calculated using a value of 125 J/g for the heat of fusion of an infinite P1B crystal.[19]

2.2. True Stress−Strain Curves. True stress−strain curves at a constant strain rate were obtained using a video-controlled tensile testing apparatus. Our apparatus is close to that developed by G'Sell[20] and was originally designed to study samples that show inhomogeneous deformation.[14] It

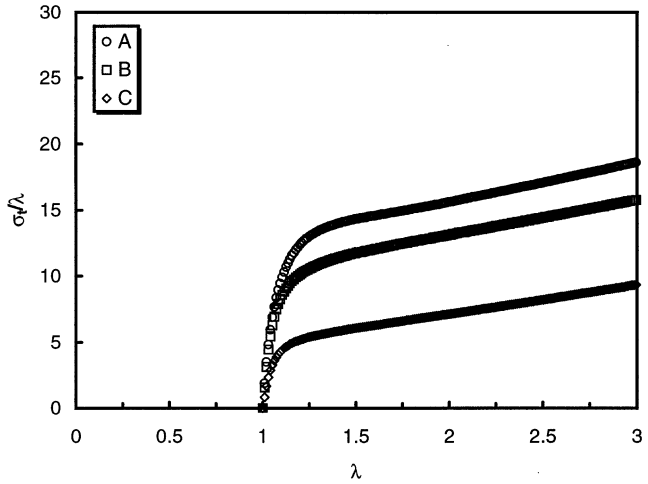

Figure 3. Associated force−extension curves of the true stress−strain curves of Figure 2.

employs a video camera connected to a computer to control the deformation of the neck by regulating the cross-head speed in a way that keeps a constant local strain rate at the center of the neck. Hencky strain was used in order to represent the true strain as given by the following equation

$$\epsilon_H = \ln \lambda \tag{1}$$

where λ is the extension ratio. Assuming a constant volume, it can be given by

$$\lambda = \frac{A_0}{A} \tag{2}$$

where A_0 and A are the initial and instantaneous cross sections, respectively. All samples were deformed uniaxially. This was checked by measuring the width-to-thickness ratio at different strains where a fairly constant value was found. For such a uniaxial test, the local Hencky strain can be extracted from the width of the test specimen following the equation

$$\epsilon_H = 2 \ln\left(\frac{w_0}{w}\right) \tag{3}$$

where w_0 and w are the initial and instantaneous widths, respectively. The true stress, σ_t, can follow also from λ and the nominal stress, σ_n

$$\sigma_t = \sigma_n \lambda = \sigma_n \exp(\epsilon_H) \tag{4}$$

Finally, the true strain rate is given by

$$\dot{\epsilon}_H = \frac{d(\ln \lambda)}{dt} \tag{5}$$

2.3. Elasticity Measurements. The same apparatus was used also to investigate the elastic−recovery properties of deformed samples at different stages of the deformation process. This was done by carrying out a step−cycle test as shown in Figure 1a. A test specimen was stretched first to a predetermined strain (ϵ_{tot}) at a constant strain rate, and then it was brought back to a zero stress using a cross-head speed of 1.95 mm/min. The remaining strain at this point represented the plastic part ϵ_{pla} of ϵ_{tot}, and the difference between the total and plastic strains gave the elastic part ϵ_{ela}. The test specimen was extended again using the same contracting cross-head speed up to the initial strain value before contracting whereupon another step was performed again under constant strain rate. This allowed the same test specimen to be used for more than one cycle (Figure 1b).

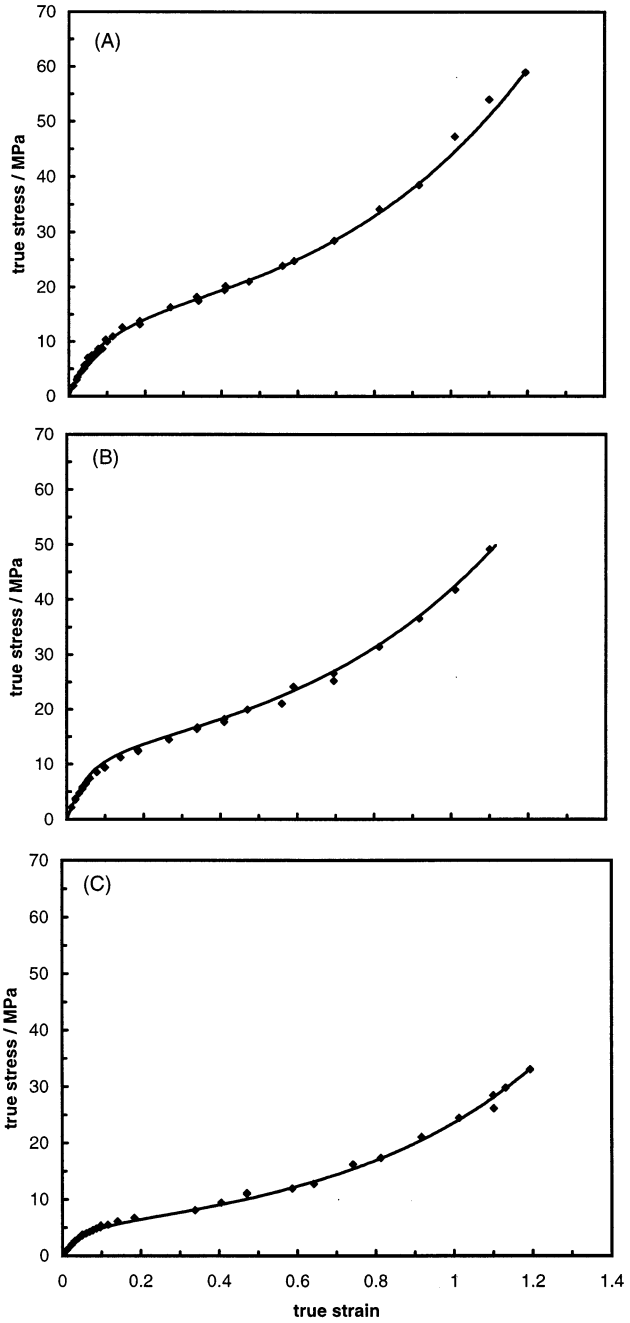

Figure 4. True stress−strain curves of the different sample (solid lines) together with the stress values after interruption during step−cycle test (the filled symbols).

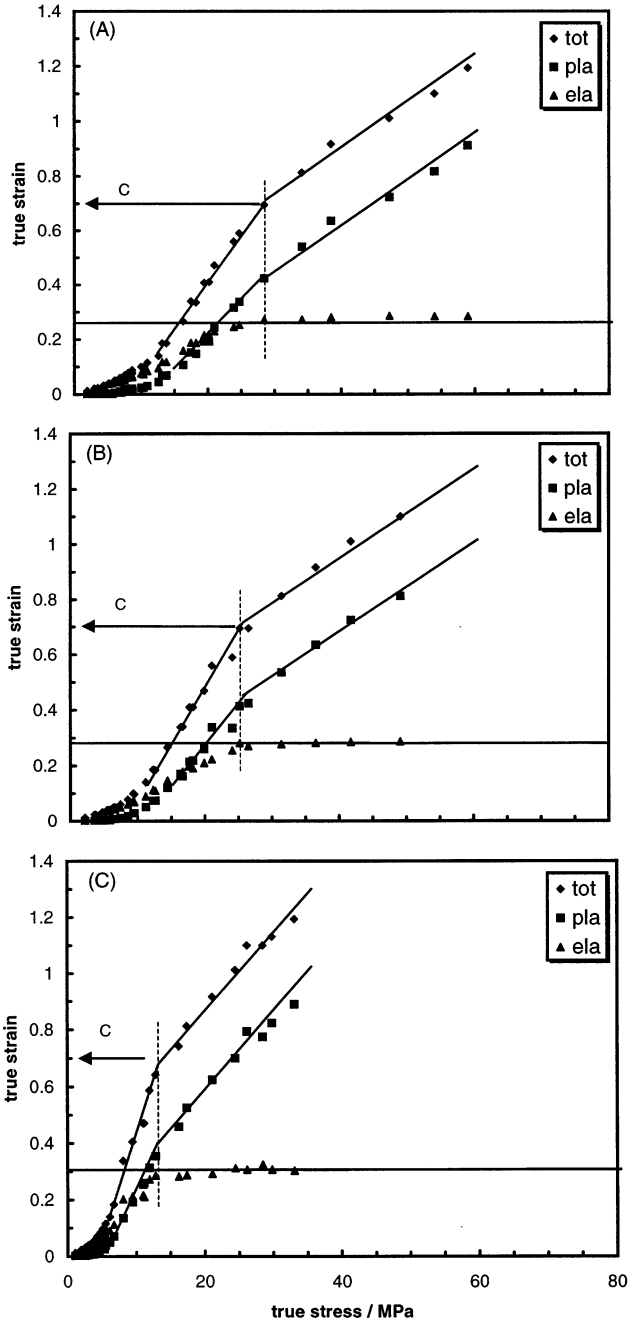

Figure 5. True total and elastic strain at different imposed true stresses for the different samples.

2.4. Wide-Angle X-ray Measurements. Wide-angle X-ray scattering (WAXS) patterns were recorded in situ in order to follow the changes in the crystalline texture at different stages of the deformation process. This was done using a rotating Cu anode generator and an image plate detector. The sample was deformed using a Mini-Instron (Rheometric Scientific Mini Mat 2000) placed between the X-ray source and the detector. A typical exposure time was 5 min.

3. Results

3.1. Deformation Behavior. Figure 2 shows true stress−strain curves obtained at a constant strain rate of 0.005 s^{-1} at room temperature for the different samples. None of the samples showed necking down during deformation despite their different crystallinities. The different curves showed a similar behavior which resembles a rubberlike elastic behavior. It started with a low initial modulus with no well-defined yield point and then followed a progressive increase in the stress until the test specimen failed. Necking does not take place until it becomes thermodynamically favorable under the deformation conditions of the experiment.[21] A mathematical description of the necking criteria is provided by Considere construction. According to this construction, necking occurs if the force−extension curve, $f(\lambda)$, showed two extreme values: a maximum and a minimum, which are located at positions where the condition $df(\lambda)/d\lambda = 0$ is fulfilled. Figure 3 shows the associated force−extension curves of the true stress−strain curves of Figure 2. As can be seen, none of the samples actually met the necking criteria. Step−cycle tests were used to decompose the imposed strain into elastic and plastic parts that were recoverable and irrecoverable, respectively, on the time scale of the

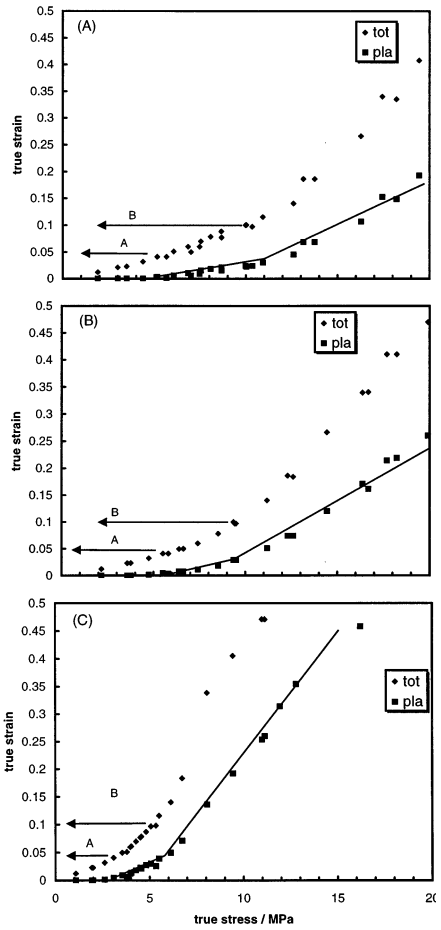

Figure 6. Low deformation region of the curves shown in Figure 5.

experiment and room temperature. In performing such a test, it is important to make sure that the interruption of each step, i.e., the contraction of the test specimen and the subsequent stretching to the initial strain value, does not cause any structural changes. If there was no structural changes, the stress value would land again at the original true stress−strain curve. This was found the case for all the different samples as shown in Figure 4. Following our previous studies, the true total, plastic, and elastic strain were plotted as a function of the true stress (Figure 5). As can be seen, at the beginning of the deformation process, both the plastic and elastic strain increased with increasing the total strain. This carried on until the total strain reached a certain value at which the elastic strain assumed a plateau value, and any further increase in the total strain proceeded by increasing the plastic strain only. Meanwhile, the slope of the drawn guide lines tended to decrease at the same point which we usually referred to as point C. This was a common behavior for all samples. The most interesting feature is that the total strain of point C was common for the different samples, ~0.7. Furthermore, looking more closely at the low deformation region revealed another two transition points, A and B, with increasing strain which occurred at the same strains of 0.05 and 0.1, respectively, for the different samples (Figure 6).

3.2. Texture Measurements. Figure 7 shows a series of typical WAXS patterns taken at different stages of deformation of sample B, as a representative example. As shown by the key pattern, the most intense reflections were the (110), (300), and (220 + 211) reflections of the stable hexagonal form I. As can be

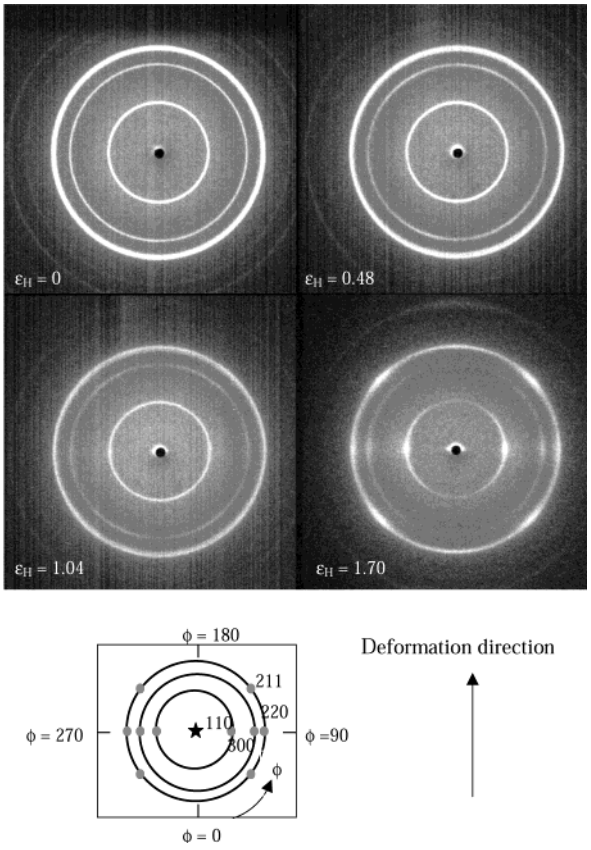

Figure 7. A series of WAXS patterns taken in situ at the indicated true strains of sample B together with a key pattern for the different reflections.

seen, the intensity distributions changed with increasing the imposed strain, indicating a change in the texture. Figure 8 shows the intensity curves of both (110) and (300) reflections at different strains. The (300) reflection developed into a four-point pattern first, and then it evolved into two sharp maxima at the equator. The (110) reflection, on the other hand, proceeded via two broad maxima on the meridian first before it evolved into another two sharp maxima on the equator. For both reflections, the strain at which the sharp maxima was observed came very near to point C strain.

4. Discussion

Coplomerization of ethylene randomly along the P1B chain resulted in a dramatic decrease in the percentage crystallinity. This gave us the opportunity to assess its influence on the deformation behavior for a set of P1B-based samples. The first apparent impact was that it correlated with the overall stress in the sense that samples with high crystallinity showed higher overall stresses. Increasing the volume fraction of the crystallites increases the internal friction, which results from inter- and intralamellar shear processes that activated during the deformation process, leading to a high overall stress. However, the different samples showed a common deformation behavior manifesting a rubberlike elasticity. Each test specimen responded as a whole to the applied stress, and no necking was observed. This made them to seem different from previous semicrystalline polymers we have studied at the beginning but that turned out not to be the case. As the deformation proceeded, both the differential compliance and the elastic properties changed at three transition points, A,

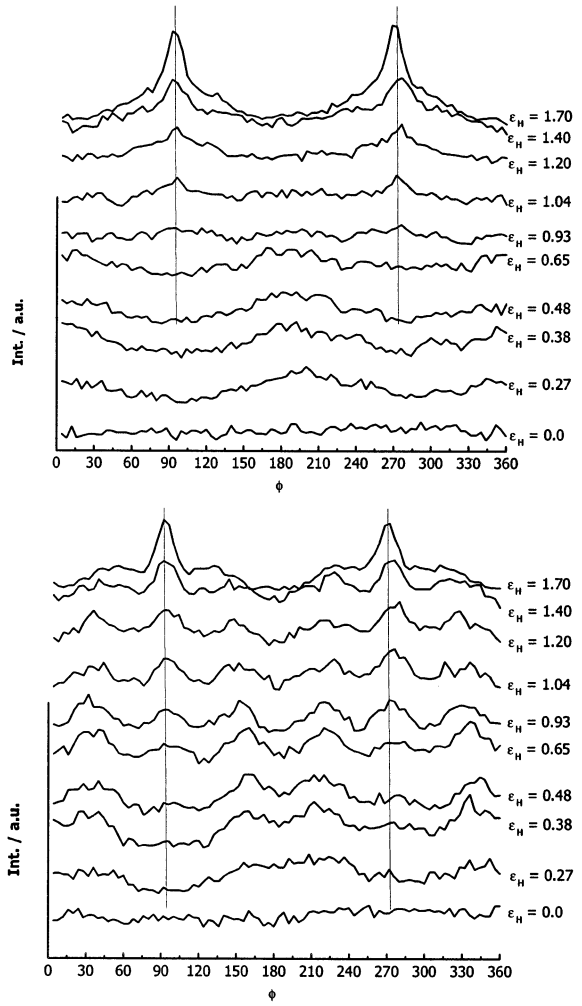

Figure 8. Intensity distribution along the azimuthal angle at the indicated true strains of (A) (110) and (B) (300) reflections.

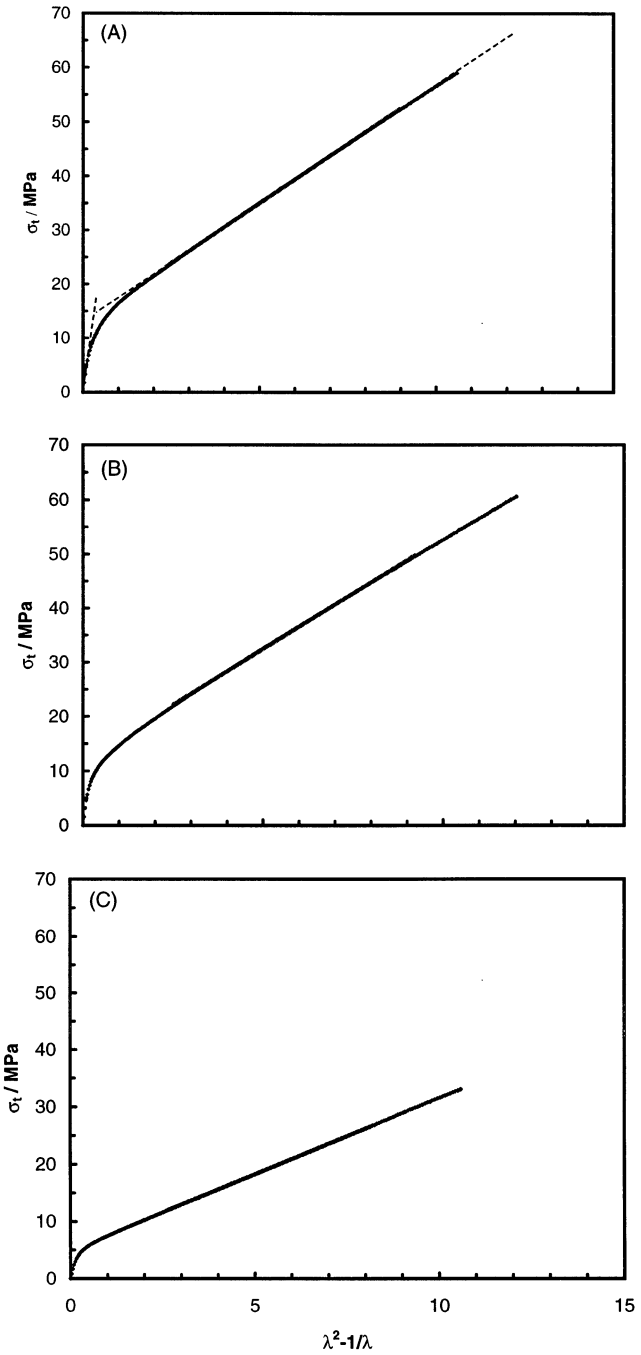

Figure 9. Plots of the true stress as a function of $\lambda^2 - 1/\lambda$ of the different samples.

B, and C, at increasing strain. A Hookean elasticity was exhibited first until point A, where a plastic strain started to occur for the first time; simultaneously, the differential compliance showed a slight increase. This continued up to point B where another more pronounced increase in the differential compliance took place. Finally, at point C the elastic strain reached a plateau value, and the differential compliance decreased this time. As the specimen was going through these points, its texture also changed correspondingly, as revealed by the WAXS patterns. It started first with a gradual increase of the molecular orientation toward the deformation direction. Then at point C sharp spots typical of a fibrillar structure appeared on the equator. Changing the crystallinity among the different samples had no effect on the strain values at which the transition points occurred along a true stress−strain curve. Once again crystallinity proved to be irrelevant for the strain-controlled deformation behavior. That the strain values of the transition points are unaffected by changing the crystallinity or other factors demonstrates the capability of semicrystalline polymers to accommodate any imposed strain in a rather well-defined way. This can only be achieved if there is a sufficient number of internal degrees of freedom available for each semicrystalline polymer by virtue of its structure. This is consistent with our recent studies of the crystallization behavior of semicrystalline polymers. We have found that the crystalline lamellae are formed via a multistep route rather than a single one.[22] It starts with the formation of an initial blocklike structure of low order out of some precursor transient mesomorphic phase which then transforms into the more stable lamellae. This leads to a granular-like lamellae rather than continuous ones, and a kind of crystalline network is formed. The chain slip processes at the boundary region between the adjacent blocks in a single lamella provide the extra needed degrees of freedom. A semicrystalline polymer can be viewed as two interpenetrating networks: the crystalline one intermingled with the entangled amorphous one. Consequently, both of these networks will contribute to any imposed deformation via inter- and interlamellar slip process. However, the extent of each contribution varies during the course of deformation.

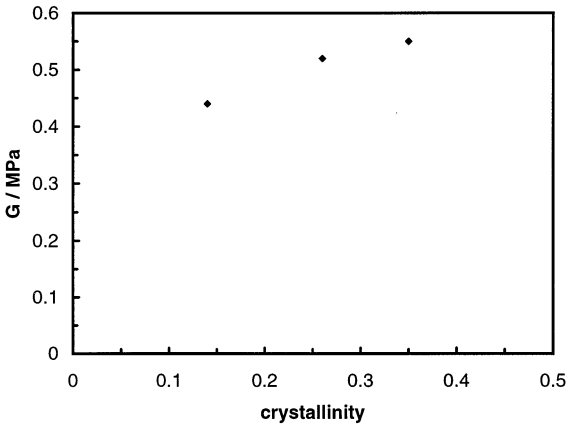

Figure 10. Network shear modulus as a function of the percentage crystallinity as extracted from Figure 9.

At low strains, the crystalline network contribution dominates through changing the coupling and invoking some coarse slips of the crystalline blocks (point B). As the strain is increased, the entangled amorphous regions becomes increasingly strained. This carries on until a critical strain is reached where the force generated from entangled fluid regions reaches a critical value that would be able to destroy the crystallites (point C). At this stage the dominant mechanism becomes the disaggregation of the crystallites and apparent recrystallization into fibrils.

Finally, the striking resemblance between the deformation behavior of the different samples and a rubber-like elasticity made it quite appealing to apply the Gaussian model of Haward and Thackray to these samples.[23,24] It is a very simple model which can be used to learn about the network properties of the different samples. According to this model, a semicrystalline polymer can be represented by a combination of a Hookean spring in series with an Eyring dashpot and a rubber elasticity spring in parallel. A plot of the true stress as a function of $\lambda^2 - 1/\lambda$ is expected to yield two lines with slopes equal to the Hookean spring elastic constant, E, and the rubber elasticity spring elastic constant, G, subsequently. The latter can be taken as the shear modulus of the effective network in the test specimen. Figure 9 shows such plots for the different samples. As can be seen, all samples showed a very good agreement with the Gaussian model. Values of G of the different samples were extracted by a linear regression of the second line. The resulting values as a function of crystallinity are shown in Figure 10. As can be seen, the network shear modulus increased with increasing the percentage crystallinity. The value of G at zero crystallinity is expected be in the order of magnitude of the melt plateau modulus, G_0. We are aware of only two published values for G_0 of the P1B melt: 0.2 MPa at 140 °C[25] and 0.14 MPa at 130 °C.[26] The extrapolated G value at zero crystallinity from Figure 10 comes in the same order of magnitude of both of these values.

5. Conclusions

The influence of the percentage crystallinity on the plastic deformation behavior of P1B-based samples was investigated. All samples showed a common general deformation behavior, whereby three characteristic transition points showed up along the true stress−strain curve. While the stresses at the three characteristic points increased with increasing the percentage crystallinity, the corresponding strains remained invariant. The WAXS measurements revealed that the microscopic texture was a function of the imposed strain. At point C the initial lamellae started to disintegrate into fibrils. This behavior is consistent with our view of a granular substructure of the crystalline lamellae. Such a blocky structure allows the polymer to respond in a well-defined manner to any imposed strain through slip processes between the blocks.

Acknowledgment. We thank Dr. Johan De Clippeleir of Basell, Louvain-La-Neuve, Belgium, for supplying us with all the materials used in this study.

References and Notes

(1) Keller, A.; Pope, D. *J. Mater. Sci.* **1971**, *6*, 453.
(2) Yamada, M.; Miyasaka, K.; Ishikawa, K. *J. Polym. Sci.* **1971**, *A-2*, 1083.
(3) Young, R.; Bowden, P.; Ritchie, J.; Rider, J. *J. Mater. Sci.* **1973**, *8*, 23.
(4) Bowden, P.; Young, R. *J. Mater. Sci.* **1974**, *9*, 2034.
(5) G'Sell, C.; Jonas, J. *J. Mater. Sci.* **1979**, *14*, 583.
(6) Seguela, R.; Rietsch, F. *J. Mater. Sci., Lett.* **1990**, *9*, 46.
(7) Bartczak, Z.; Argon, A. S.; Cohen, R. E. *Macromolecules* **1992**, *25*, 5036.
(8) Brooks, N. W.; Duckett, R. A.; Ward, I. M. *Polymer* **1992**, *33*, 1872.
(9) Ciferri, A.; Ward, I. M. *Ultar-high Modulus Polymers*; Applied Science: London, 1977.
(10) Capaccio, G.; Compton, T. A.; Ward, I. M. *J. Polym. Sci., Phys.* **1976**, *14*, 1641.
(11) Al-Hussein, M.; Davies, G. R.; Ward, I. M. *Polymer* **2001**, *42*, 3679.
(12) Hobeika, S.; Men, Y.; Strobl, G. *Macromolecules* **2000**, *33*, 1827.
(13) Men, Y.; Strobl, G. *J. Macromol. Sci., Phys.* **2001**, *40*, 775.
(14) Hiss, R.; Hobeika, S.; Lynn, C.; Strobl, G. *Macromolecules* **1998**, *32*, 4390.
(15) Lindegren, C. R. *Polym. Eng. Sci.* **1970**, *10*, 163.
(16) Kemp, S. G. *Plast. Rubb. Process. Appl.* **1983**, *3*, 169.
(17) Weynant, E.; Haudin, J. M.; G'Sell, C. *J. Mater. Sci.* **1982**, *17*, 1017.
(18) Yang, Y.; Geil, P. *Makromol. Chem.* **1985**, *186*, 1961.
(19) ATHAS Data Bank http://web.utk.edu/athas/datanbank.
(20) G'Sell, C.; Hiver, J. M.; Dahoun, A.; Souahi, A. *J. Mater. Sci.* **1992**, *27*, 5031.
(21) Strobl, G. *The Physics of Polymers*; Springer: Berlin, 1996.
(22) Strobl, G. *Eur. Phys. J. E* **2001**, *3*, 165.
(23) Haward, R.; Thackray, G. *Proc. R. Soc. London, A* **1968**, *302*, 453.
(24) Haward, R. *Macromolecules* **1993**, *26*, 5860.
(25) Fetters, L. J.; Lohse, D. J.; Richter, D.; Witten, D. A.; Zirkel, A. *Macromolecules* **1994**, *27*, 4639.
(26) Friedrich, Chr.; Eckstein, A.; Stricker, F.; Muelhaupt, R. In *Rheology and Peocessing of Metallocene-based Polyolefines in Metallocene-based polyolefines: Preparation, Properties and Technology*; Sheirs, J., Kamainski, W., Eds.; Wiley: New York, 2000.

MA020831K